2015

Terrestrial Laser Scanning Roughness Assessments for Infrastructure

Ahmad A. Alhasan
Iowa State University, aalhasan@iastate.edu

David J. White
Iowa State University, djwhite@iastate.edu

Terrestrial Laser Scanning Roughness Assessments for Infrastructure

Ahmad Alhasan
Department of Civil, Construction and Environmental Engineering
Iowa State University
394 Town Engineering Building
Ames, IA 50011-3232
Email: aalhasan@iastate.edu

David J. White, Ph.D., P.E.
Department of Civil, Construction and Environmental Engineering
Iowa State University
422 Town Engineering Building
Ames, IA USA 50011-3232
Email: djwhite@iastate.edu

ABSTRACT

Road roughness is a key parameter for controlling pavement construction processes and for assessing ride quality of both paved and unpaved roads. This paper describes algorithms used in processing three-dimensional (3D) stationary terrestrial laser scanning (STLS) point clouds to obtain surface maps of point wise indices that characterize pavement roughness. The backbone of the analysis is a quarter-car model simulation over a spatial 3D mesh grid representing the pavement surface. Two case studies are presented, and results show high spatial variability in the roughness indices both longitudinally and transversely (i.e., different wheel path positions). It is proposed that road roughness characterization using a spatial framework provides more details on the severity and location of roughness features compared to the one-dimensional methods. This paper describes approaches that provide an algorithmic framework for others collecting similar STLS 3D spatial data to be used in advanced road roughness characterization.

Keywords: 3D laser Scanning—road roughness—algorithms

INTRODUCTION

Road surface roughness increases vehicle operation and travel delay costs (Gao and Zhang 2013; Ouyang and Madanat 2004); reduces vehicle durability (Bogsjö and Rychlik 2009; Oijer and Edlund 2004); and reduces ride quality and structural performance (Al-Omari and Darter 1994). Structural performance diminishes faster on rough roads because rough features increase dynamic stresses that accelerate structural deterioration (Lin et al. 2003). Accurate evaluation of pavement roughness levels and modes is a key factor in optimizing maintenance decisions (Chootinan et al. 2006; Kilpeläinen et al. 2011; Lamptey et al. 2008) and a leading indicator in construction quality assurance/quality control (QC/QA).

In 1986, the International Roughness Index (IRI) was introduced as a time stable pavement roughness measurement (Sayers et al. 1986; Sayers et al. 1986). Since then IRI has been widely used because it empirically correlates with ride quality and vehicle operating costs (Gao

Proceedings of the 2015 Conference on Autonomous and Robotic Construction of Infrastructure, Ames, Iowa.

and Zhang 2013; Ouyang and Madanat 2004; Tsunokawa and Schofer 1994). IRI is calculated by mathematically simulating the quarter-car dynamics and accumulating the quarter-car suspension response induced by variations in a vertical profile. Current teste method for measuring longitudinal profiles using an inertial profiler (ASTM E950 / E950M-09) is most suited for collecting data in one or two or even few profiles, however it is hard to synchronize these profiles to test the transverse variability in elevation at a specific point. Karamihas et al. (1999) investigated the variability in the IRI values for different profiles across the road, and reported that two profiles across the lane are not representative of the entire lane and that drivers typical wander laterally within a range of 50 cm (20 in).

Another limitation when reporting summary indices with fixed analysis interval, is the ability to detect localized features, Swan and Karamihas (2003) proposed reporting IRI continuously by applying a moving average to the suspension response. Studies have shown that local features affect rider comfort, pavement stresses, and cause most vehicle fatigue damage (Bogsjö and Rychlik 2009; Kuo et al. 2011; Oijer and Edlund 2004; Steinwolf et al. 2002).

Unlike paved roads, there is a lack of a common set of criteria to evaluate unpaved roads, many local agencies use visual inspection to estimate an IRI value (Archondo-Callao 1999; Namur and de Solminihac 2009; Walker et al. 2002). Some agencies combine visual inspection with direct measurement of defects (e.g., pothole depth, corrugation spacing) (Soria and Fontenele 2003; Woll et al. 2008). Several studies have pointed out the importance of precise assessment of unpaved road conditions using indirect data acquisition methods such as unmanned aerial vehicles (UAV), ground penetrating radar (GPR), and accelerometers to help transportation agencies decide whether to maintain or upgrade these roads (Berthelot et al. 2008; Brown et al. 2003; Zhang 2009; Zhang and Elaksher 2012).

Recent developments in laser scanning techniques and light detection and ranging (LIDAR) sensing have motivated researchers and practitioners to adopt these technologies due to the accurate and rich data measurements. Recent studies (Fu et al. 2013; Tsai et al. 2010; Zalama et al. 2011) have demonstrated the effectiveness of laser scanning and LIDAR in identifying geometrical features of interest (e.g., cracks, bumps). Also, recent studies have investigated the applicability of using stationary three dimensional (3D) laser scanning techniques in obtaining IRI by selectively extracting track profiles (Chang and Chang 2006) or by analyzing the surface to develop spatial roughness maps (Alhasan et al. 2015).

This study will introduce an overview of stationary laser scanning approach and the practical needs for applications in road roughness assessment. Also a discussion of a procedure and associated algorithms that can be used in processing 3D point clouds obtained for paved and unpaved sections, to obtain spatial surface maps of rectified slopes (RS) and IRI values across road sections. A brief review of frequency based analysis (i.e. Fast Fourier transform, FFT and Continues wavelet transform) will be introduced as well. Frequency based approaches can reveal the sources of road roughness. The backbone of the analysis approaches described herein is a quarter-car model.

DATA COLLECTION USING STATIONARY LASER SCANNER

LIDAR systems measure information (spatial coordinates and color) of a 3D space and store the information in a 3D point cloud. The term LIDAR is generic, and includes airborne laser scanning technologies, mobile scanners mounted on vehicles, and stationary laser scanners or stationary terrestrial laser scanners (STLS), where the laser scanner is fixed at a station with

known coordinates and based on the distance between the scanner and the detected points, a geospatially referenced 3D point cloud is constructed. Trimble CX 3D STLS system was used in two case studies to acquire 3D laser scans. The position accuracy of a single point is 4.5 mm at 30 m and drops to 7.3 mm at 50 m. The distance accuracy is 1.2 mm at 30 m and drops to 2 mm at 50 m. Figure 1 shows the scanner set-up.

Figure 1. Trimble CX 3D laser scanner set-up.

Scanning process starts by acquiring full scan that covers the 360° x 300° view. This scan produces a mother file that includes common targets (Figure 2) to be used for registration in the post processing. Area scans are then conducted to acquire denser point clouds for the areas of interest. The size of the targets affect the density of the full scan, where smaller targets require high density full scans to capture them. However, the density of the area scans can vary depending on the application. In the two case studies, criterion specified to analyze roads roughness from the point cloud was a maximum spacing of 100 mm in both spatial directions (longitudinal and transverse) between two consecutive points in the region of interest. By several trials it was found that a density of 35 mm at 100,000 mm for the area scans produced sufficiently dense clouds to satisfy the 100 mm spacing criterion.

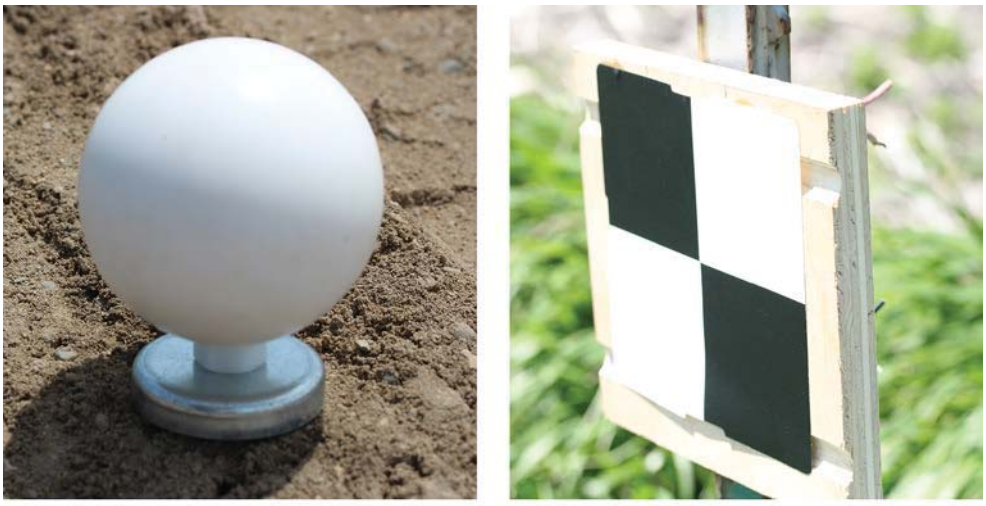

Figure 2. Reference point (a) spherical targets and (b) flat black and white target.

After acquiring the data, the scan should be registered in a specialized software. Many activities can be performed using software packages, such as registration, fitting geometries. Registration of clouds is done by identifying common targets (spheres or flat targets as shown in Figure 2) appearing in the full scans of each consecutive station that share a common spatial domain with other stations. These targets are used as benchmarks to geospatially reference scans by matching the common target locations in each scan, and thus stitching the scans to produce a full 3D cloud. Figure 3 shows examples of the registered point clouds. The variation in color indicates the material reflectivity.

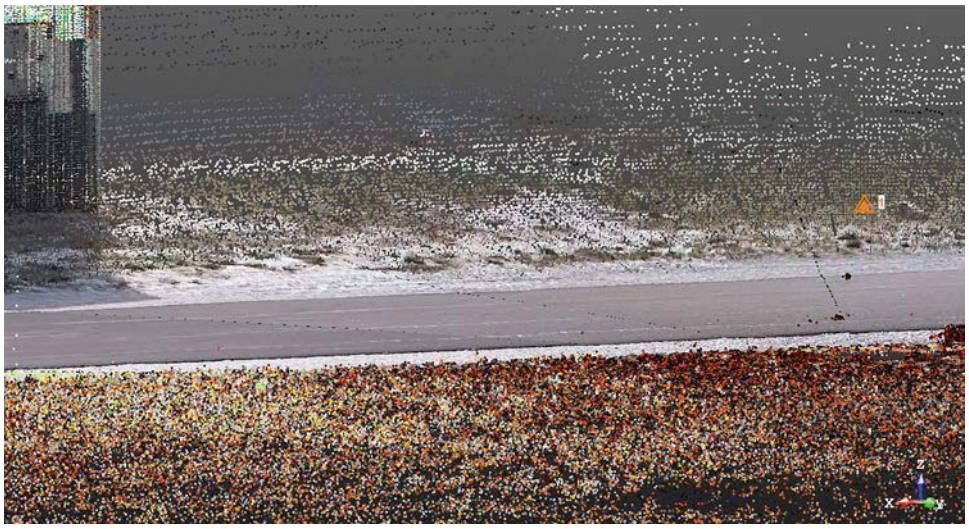

Figure 3. Registered point cloud.

After registration, the point clouds are cleaned of unnecessary data points, where the sections of interest should be separated from areas beyond the edges of the sections and noise from any passing vehicles that might appear in the scans. The final data points left after cleaning can be

exported in ASCII file format; these files contain the x, y, and z coordinates of the points in the section under consideration.

DATA PROCESSING

Visioning Algorithms

To use the road surface in simulations developed algorithms require a uniformly spaced grid the longitudinal direction. To achieve that a mesh grid is formed with grid elements that have a predefined *x* and *y* edge dimensions. The grid centre elevation is calculated as the average of all cloud points falling in that grid region. All points are rotated and translated to a local coordinate system corresponding to the longitudinal and transvers axes (Zalama et al. 2011). Transformation for processing along horizontal curves can be achieved by constructing a curvilinear local coordinate system; however, for simple geometries without curves the point cloud is rotated globally, where the x axis corresponds to the longitudinal direction and the y axis to the transverse direction. Vertical slopes are corrected by subtracting the z elevation along a quadratic fit from the *z* coordinate of the corresponding transformed points (Alhasan et al. 2015). Figure 4 shows a pavement section point cloud data after processing in the visioning algorithm.

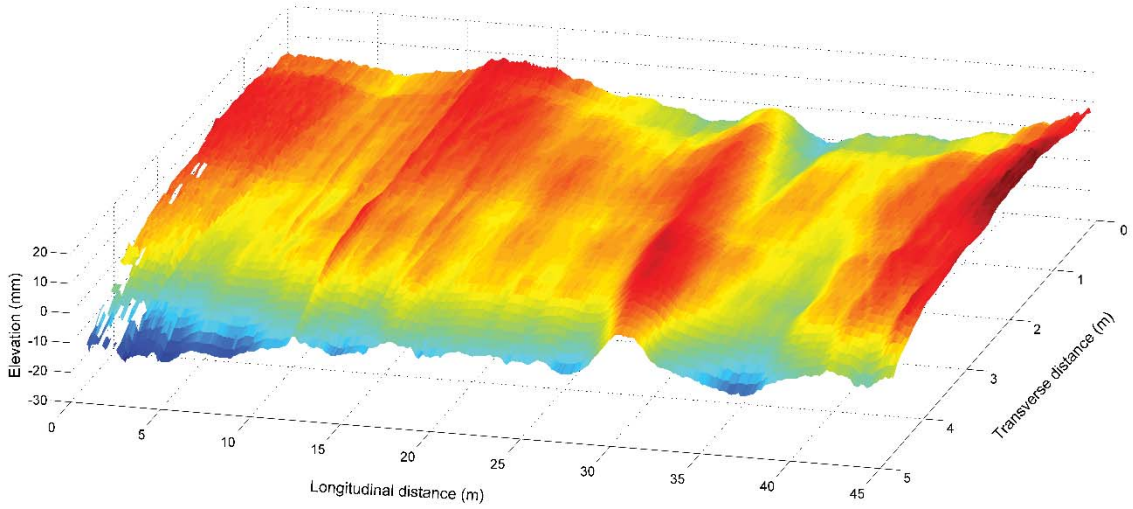

Figure 4. Point cloud data after processing in the visioning algorithm for a pavement section.

Roughness Evaluation Algorithms

Evaluation of roughness described herein is based on the responses of the quarter-car model described in (ASTM E1926-08). Figure 5 presents a schematic of the quarter-car model. Where M_s and M_u are the sprung and unsprung masses respectively, k_s and k_t are the suspension and tire spring coefficients respectively, and c_s is the suspension damping rate.

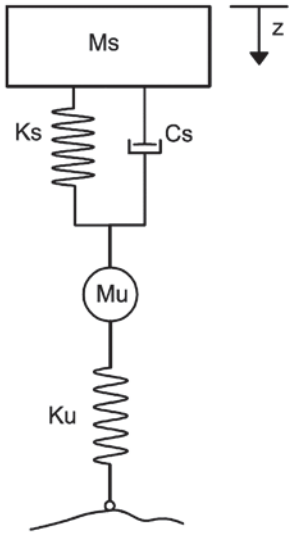

Figure 5. Quarter-car model.

The dynamics of the system can be described by four first-order differential equations presented in a matrix form (Sayers and Karamihas 1996) (Equations 1—4):

$$\dot{X} = AX + B\,h_{ps} \tag{1}$$

Where;

$$X = \begin{bmatrix} z_S & \dot{z}_S & z_u & \dot{z}_u \end{bmatrix}^T \tag{2}$$

$$A = \begin{bmatrix} 0 & 1 & 0 & 0 \\ -k_2 & -c & k_2 & c \\ 0 & 0 & 0 & 1 \\ \frac{k_2}{\mu} & \frac{c}{\mu} & -\frac{(k_1+k_2)}{\mu} & -\frac{c}{\mu} \end{bmatrix} \tag{3}$$

$$B = \begin{bmatrix} 0 & 0 & 0 & k1/\mu \end{bmatrix}^T \tag{4}$$

Where h_{ps} is the elevation of the profile after applying the moving average smoother; z_S and z_u are the elevations of sprung and unsprung masses; $\dot{z}_S$ and $\dot{z}_u$ are elevation time derivatives of sprung and unsprung masses; k_1 is the tire spring coefficient divided by the sprung mass, k_2 is

the suspension spring coefficient divided by the sprung mass, *c* is the suspension damping rate divided by the sprung mass, and μ is the ratio of unsprung to sprung mass. Two approaches can be followed to solve this system, a finite difference solution that solves the system in stepwise fashion and a frequency domain solution (Fourier analysis). The outcome of the solution is the rectified slope profile, which is the time rate at which the sprung mass is moving in the z direction relative to the unsprung mass. This index reflects the suspension rate for a quarter-car model.

Finite Difference Algorithms

The differential equation described in Equation 1 can be solved in state-space form as shown Equation 5 (Murray et al. 1994; Sayers and Karamihas 1996). FORTRAN code is provided in (ASTM E1926-08) to solve this system. The code can be translated to MATLAB code and used to simulate the quarter-car model over each longitudinal strip in the grid developed from the point cloud. A longitudinal strip is defined as a sequence of grid elements in the x direction having one y coordinate. The longitudinal strips are used as an input profile for simulations. This approach leads to a surface roughness map where the rectified slope is a function of the variable *x* and the fixed coordinate *y*. Because each profile is simulated independently, transverse effects such as rolling and pitch are not included.

$$X_i = S\,X_{i-1} + P\,h_{ps} \tag{5}$$

Where;

$$S = e^{A\Delta x/v}$$

$$P = A^{-1}(S - I)B \tag{6}$$

X, *A*, h_{ps}, and *B* are predefined in Equations 1—4, Δx is the spacing between profile points, *v* is the assumed speed of the model, and *I* is the identity matrix. The finite difference algorithm is implemented in many commercial packages and proved efficiency when used in analysing long profiles. However, the algorithm suffers from long memory effects, where the rectified slope at a point is affected by the elevation of previous points back to several meters, reaching 10 meters in some cases, and thus the starting point affects the results when analysing short profiles (Swan and Karamihas 2003). The critical length of the profile depends on several factors, the smoothness of the profile to be analysed and the sampling frequency of the data acquisition system.

Frequency domain algorithms

Frequency analysis is another approach to solve the described dynamic system. This approach namely depends on transforming the state equations from spatial to frequency or quasi-frequency domain. The analytical description of quarter-car model is best explained in terms of random signal analysis, where fast Fourier transformation (FFT) can be a helpful tool for such analysis. The basic assumption in this approach is that any profile can be decomposed into building sinusoids, for infinite precision the signal should be decomposed to an infinite number of sinusoids, however only finite number can be used to describe a signal. Results for the FFT analysis can be characterized by examining the height amplitude versus spatial frequency plots (Alhasan et al. 2015), or by applying a band-pass filter (Liu and Herman 1999) that characterizes the analytical solution of the quarter car model in frequency domain, this filter results in rectified slope profile.

Wavelet analysis techniques were developed independently in different fields (i.e., pure mathematics, physics, and engineering) to overcome the time-frequency resolution issue in Fourier analysis (Boggess and Narcowich 2009; Daubechies 1992). This issue results from the assumption that sines and cosines, which are infinitely periodic functions, are building blocks for any function. This assumption induces uncertainty in the analysis, where high resolution cannot be achieved simultaneously in both frequency and space domains. Wavelets, which can be thought of as wave pulses that translate in the spatial domain and can change size (i.e., dilate or shrink), are used as building blocks to overcome the time-frequency resolution issue. Wavelets come in families, and for each family there is a wavelet, the "mother wavelet," and a scaling function, a "father wavelet," although some families do not include scaling functions. Wavelet dispersion is controlled by a scale factor 'a', where larger scale factors correspond to dilated waves and smaller scale factors correspond to shrunken waves.

Wavelet transform projects (transforms) the profile on a wavelet function at different scales (layers of details) to result in wavelet coefficients describing the correlation between the signal and the wavelet function. This decomposition allows examining the location of features with certain frequency bands with known effect on vehicle response, and thus provides a valuable tool to determine localized features (Alhasan et al. 2015).

CASE STUDIES

Road roughness of two road sections was evaluated, the sections include a 55 m long rural unpaved road and a 58.8 m long HMA overlay over a jointed plain concrete pavement (JPCP) pavement. Figures 6a and 6b show the rectified slope map for rural road and the paved road respectively.

For the unpaved road the left lane extends between stations 0 and 3 in the transverse distance, and the right lane extends between stations 0 and -3. This map reveals great details, for instance the central region is unsystematically rough compared to the rest of the scan area, however a localized rough region appears in the left lane between stations 50 and 55, which corresponds to a loose pile of aggregate. The paved road surface map includes an approximately 3 m wide lane that extends between stations 0 and 4. The map shows the severity and location of the reflective cracks in the transvers direction.

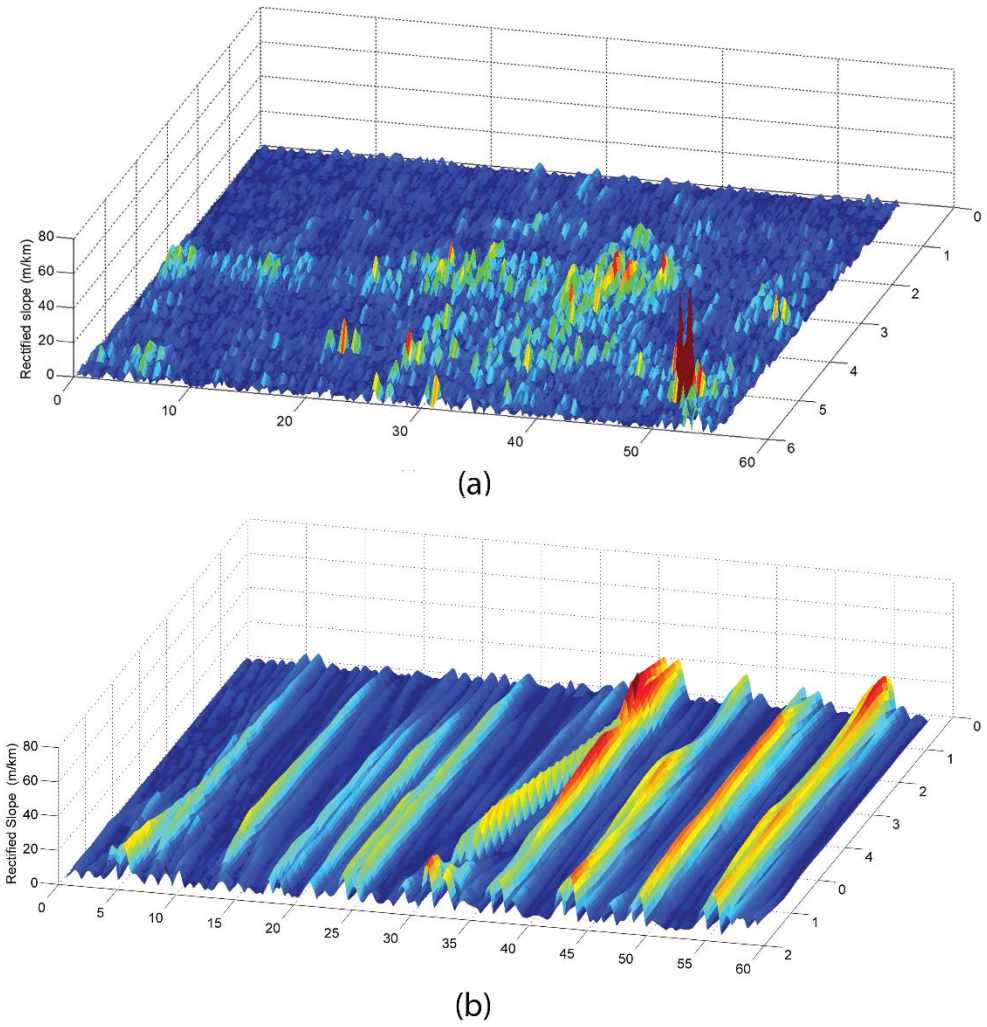

Figure 6. Absolute rectified slope surface maps for (a) unpaved and (b) paved roads.

The average of rectified slope values along each profile is defined as its IRI, since the map was generated by simulating a quarter-car model moving at a speed of 80 km/h. Figure 7 shows the IRI values versus width for both roads, it can be noticed that IRI values are highly variable. Due to the high variability in IRI values it is proposed to base the conclusions regarding surface roughness on the IRI versus width plots, and if a single summary index is needed median would be a more proper way to report overall IRI values than the average. The advantage of using the median is robustness to outliers.

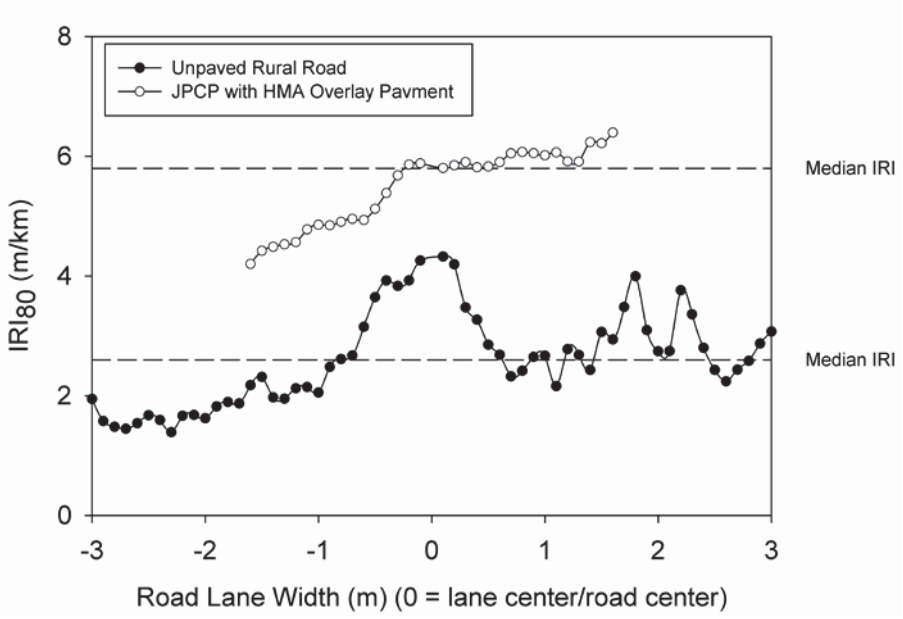

Figure 7. IRI versus width for both road sections included in the study.

To investigate the reason for low IRI values for the unpaved section, two profiles were transformed to frequency space, one profile corresponding to maximum IRI value and another profile corresponding to minimum IRI value. Each profile was decomposed into its constituent spectrum using the FFT (Figure 8). Presenting the results as height amplitude versus spatial frequency clearly shows different components of amplitude and frequency. The threshold for "smooth" was set at amplitude less than 0.4 mm. "Unsystematically rough" is defines as amplitude greater than 0.4 mm, but variable over a range of spatial frequencies. "Corrugation" is defined as amplitude with a central peak of greater than 0.7 mm and a spatial frequency of 1.5 to 2.5 (1/m). By examining the results this way, the source of roughness can be distinguished. And it can be seen that highest amplitudes are due to corrugations, however the quarter-car filter attenuates these frequencies, which results in substantially lower IRI values.

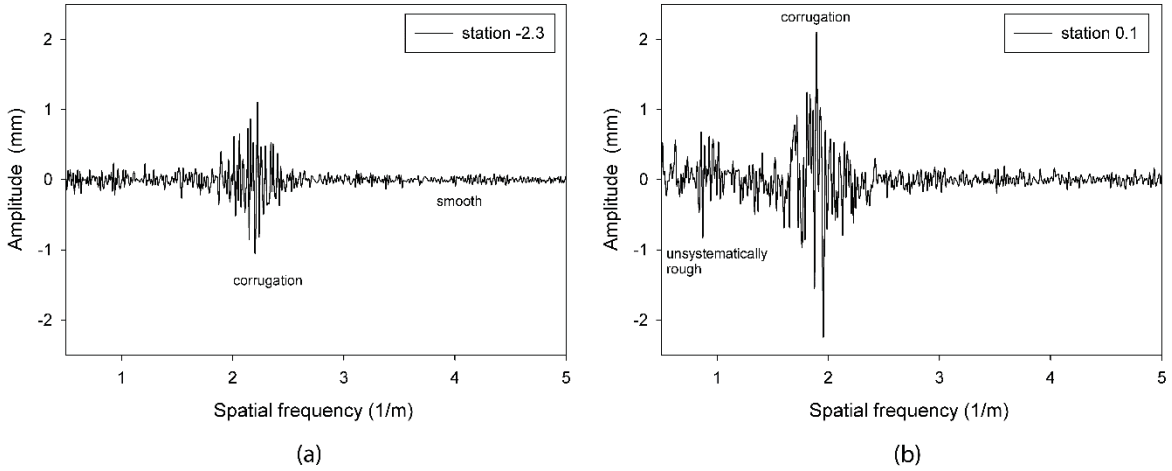

Figure 8. FFT for road profiles in (a) smooth surface with corrugations, (b) unsystematically rough surface with corrugations.

SUMMARY AND CONLUSIONS

This paper introduces the frame work of quantitative techniques for evaluating the surface roughness of paved and unpaved roads. Methods for evaluating the surface roughness can be set to two main categories, finite difference simulation and frequency domain analysis. The key findings from this research are:

- Terrestrial laser scanning is a promising technology to assess a range of surface conditions for unpaved roads.
- 2-D Surface roughness maps were developed using the information obtained from the laser scanner.
- Algorithms used in producing 2-D roughness maps are semi-automated, and further developments are expected to introduce fully automated algorithms that can process the data directly after scanning.
- IRI values are highly variable across the road section, thus it is hard to define the appropriate profile to be used as the representative profile.
- The proposed analysis technique can be used to identify localized rough features.
- Finite difference simulations are not suitable for short profiles.
- Filtering of the profiles in Fourier space as a tool to get the spatial roughness maps are more suitable compared to finite difference algorithms for analyzing short profiles, however wavelet analysis provide a more robust approach to analyze short profiles and identify localized features.
- At this stage, high resolution terrestrial laser scans are time consuming and require trained personnel; however, newer terrestrial laser scanners will be able to reduce the data acquisition time significantly due to faster scanning rates and longer ranges.

REFERENCES

ProVAL: Profile Viewing and Analysis Software, version 3.4 (2013),The Transtec Group, Inc. available from www.RoadProfile.com.

Al-Omari, B., and Darter, M. I. (1994). "Relationships between international roughness index and present serviceability rating." *Transportation Research Record*(1435).

Alhasan, A., White, D. J., and De Brabanter, K. (2015). "Continuous wavelet analysis of pavement profiles." *Automation in Construction*, Under review.

Alhasan, A., White, D. J., and De Brabanter, K. (2015). "Quantifying Unpaved Road Roughness from Terrestrial Laser Scanning." *2015 TRB 94th Annual Meeting*Washington, D.C.

Alhasan, A., White, D. J., and De Brabanter, K. (2015). "Spatial pavement roughness from stationary laser scanning." *International Journal of Pavement Engineering*, Under review.

Archondo-Callao, R. (1999). "Unpaved roads roughness estimation by subjective evaluation." *The World Bank*.

ASTM E950 / E950M-09 "Standard Test Method for Measuring the Longitudinal Profile of Traveled Surfaces with an Accelerometer Established Inertial Profiling Reference."ASTM International, West Conshohocken, PA, 2008, www.astm.org.

ASTM E1926-08 "Standard Practice for Computing International Roughness Index of Roads from Longitudinal Profile Measurements."ASTM International, West Conshohocken, PA, 2008, www.astm.org.

Berthelot, C. F., Podborochynski, D., Stuber, E., Prang, C., and Marjerison, B. (2008). "Saskatchewan Case Studies of Network and Project Level Applications of a Structural Asset Management System." *Proc., 7th International Conference on Managing Pavement Assets. TRB Committee AFD10 on Pavement Management Systems, Transportation Research Board, Washington, DC Retrieved October*, 2011.

Boggess, A., and Narcowich, F. J. (2009). *A first course in wavelets with Fourier analysis*, John Wiley & Sons.
Bogsjö, K., and Rychlik, I. (2009). "Vehicle fatigue damage caused by road irregularities." *Fatigue & Fracture of Engineering Materials & Structures*, 32(5), 391-402.
Brown, M., Mercier, S., and Provencher, Y. (2003). "Road maintenance with Opti-Grade®: Maintaining road networks to achieve the best value." *Transportation Research Record: Journal of the Transportation Research Board*, 1819(1), 282-286.
Chang, J.-R., and Chang, K.-T. (2006). "Application of 3 D laser scanning on measuring pavement roughness." *ASTM Journal of Testing and Evaluation*, 34(2), 83-91.
Chootinan, P., Chen, A., Horrocks, M. R., and Bolling, D. (2006). "A multi-year pavement maintenance program using a stochastic simulation-based genetic algorithm approach." *Transportation Research Part A: Policy and Practice*, 40(9), 725-743.
Daubechies, I. (1992). *Ten lectures on wavelets*, SIAM.
Fu, P., Lea, J. D., Lee, J. N., and Harvey, J. T. (2013). "Comprehensive evaluation of automated pavement condition survey service providers' technical competence." *International Journal of Pavement Engineering*, 14(1), 36-49.
Gao, H., and Zhang, X. (2013). "A Markov-Based Road Maintenance Optimization Model Considering User Costs." *Computer-Aided Civil and Infrastructure Engineering*, 28(6), 451-464.
Karamihas, S. M., Gillespie, T. D., Kohn, S. D., and Perera, R. W. (1999). "Guidelines for longitudinal pavement profile measurement: final report." 126p + appendices.
Kilpeläinen, P., Jaakkola, M., and Alanaatu, P. (2011). "Development of a control system for a multipurpose road repairing machine." *Automation in Construction*, 20(6), 662-668.
Kuo, C. M., Fu, C. R., and Chen, K. Y. (2011). "Effects of Pavement Roughness on Rigid Pavement Stress." *Journal of Mechanics*, 27(1), 1-8.
Lamptey, G., Labi, S., and Li, Z. (2008). "Decision support for optimal scheduling of highway pavement preventive maintenance within resurfacing cycle." *Decision Support Systems*, 46(1), 376-387.
Lin, J.-D., Yau, J.-T., and Hsiao, L.-H. (2003). "Correlation analysis between international roughness index (IRI) and pavement distress by neural network." *Proc., 82nd annual meeting in January, 2003*.
Liu, C., and Herman, R. (1999). "Road profile, vehicle dynamics, and ride quality rating." *Journal of transportation engineering*, 125(2), 123-128.
Murray, R. M., Li, Z., Sastry, S. S., and Sastry, S. S. (1994). *A mathematical introduction to robotic manipulation*, CRC press.
Namur, E., and de Solminihac, H. (2009). "Roughness of Unpaved Roads Estimation and Use as an Intervention Threshold." *Transp. Res. Record*(2101), 10-16.
Oijer, F., and Edlund, S. (2004). "Identification of transient road obstacle distributions and their impact on vehicle durability and driver comfort." *Vehicle System Dynamics*, 41, 744-753.
Ouyang, Y., and Madanat, S. (2004). "Optimal scheduling of rehabilitation activities for multiple pavement facilities: exact and approximate solutions." *Transportation Research Part A: Policy and Practice*, 38(5), 347-365.
Sayers, M. W., Gillespie, T. D., and Paterson, W. D. (1986). *Guidelines for conducting and calibrating road roughness measurements*.
Sayers, M. W., Gillespie, T. D., and Queiroz, A. (1986). "The international road roughness experiment. Establishing correlation and a calibration standard for measurements."
Sayers, M. W., and Karamihas, S. M. (1996). "Interpretation of road roughness profile data."
Sayers, M. W., and Karamihas, S. M. (1996). "Interpretation of road roughness profile data." University of Michigan Transportation Research Institute.

Soria, M., and Fontenele, E. (2003). "Field Evaluation of Method for Rating Unsurfaced Road Conditions." *Transportation Research Record: Journal of the Transportation Research Board*, 1819(-1), 267-272.

Steinwolf, A., Giacomin, J., and Staszewski, W. (2002). "On the need for bump event correction in vibration test profiles representing road excitations in automobiles." *Proceedings of the Institution of Mechanical Engineers, Part D: Journal of Automobile Engineering*, 216(4), 279-295.

Swan, M., and Karamihas, S. M. (2003). "Use of a ride quality index for construction quality control and acceptance specifications." *Transportation Research Record*(1861), p. 10-16.

Tsai, Y. J., Wu, J., Wang, Z., and Hu, Z. (2010). "Horizontal roadway curvature computation algorithm using vision technology." *Computer-Aided Civil and Infrastructure Engineering*, 25(2), 78-88.

Tsunokawa, K., and Schofer, J. L. (1994). "Trend curve optimal control model for highway pavement maintenance: Case study and evaluation." *Transportation Research Part A: Policy and Practice*, 28(2), 151-166.

Walker, D., Entine, L., and Kummer, S. (2002). "Gravel-Paser Manual: Pavement Surface Evaluation and Rating." Wisconsin Transportation Information Center.

Woll, J. H., Surdahl, R. W., Everett, R., and Andresen, R. (2008). "Road Stabilizer Product Performance: Seedskadee National Wildlife Refuge." Federal Highway Administration.

Zalama, E., Gómez-García-Bermejo, J., Llamas, J., and Medina, R. (2011). "An effective texture mapping approach for 3D models obtained from laser scanner data to building documentation." *Computer-Aided Civil and Infrastructure Engineering*, 26(5), 381-392.

Zhang, C. (2009). "Monitoring the Condition of Unpaved Roads with Remote Sensing and Other Technology." Geographic Information Science Center of Excellence, South Dakota State University.

Zhang, C., and Elaksher, A. (2012). "An Unmanned Aerial Vehicle-Based Imaging System for 3D Measurement of Unpaved Road Surface Distresses1." *Computer-Aided Civil and Infrastructure Engineering*, 27(2), 118-129.